2013

MODIS-derived spatiotemporal water clarity patterns in optically shallow Florida Keys waters: A new approach to remove bottom contamination

Brian B. Barnes
University of South Florida, bbarnes4@mail.usf.edu

Chuanmin Hu
University of South Florida

Blake A. Schaeffer
US-EPA

Zhongping Lee
University of Massachusetts

David A. Palandro
Florida Fish and Wildlife Conservation Commission

See next page for additional authors

Remote Sensing of Environment 134 (2013) 377–391

Contents lists available at SciVerse ScienceDirect

Remote Sensing of Environment

journal homepage: www.elsevier.com/locate/rse

MODIS-derived spatiotemporal water clarity patterns in optically shallow Florida Keys waters: A new approach to remove bottom contamination

Brian B. Barnes [a,*], Chuanmin Hu [a], Blake A. Schaeffer [b], Zhongping Lee [c], David A. Palandro [d,e], John C. Lehrter [b]

[a] College of Marine Science, University of South Florida, 140 7th Avenue South, St. Petersburg, FL, 33701, USA
[b] National Health and Environmental Effects Research Laboratory, Gulf Ecology Division, United States Environmental Protection Agency, Gulf Breeze, FL, USA
[c] School for the Environment, University of Massachusetts, Boston, MA, USA
[d] Fish and Wildlife Research Institute, Florida Fish and Wildlife Conservation Commission, St. Petersburg, FL, USA
[e] ExxonMobil Upstream Research Company, Houston, TX, USA

ARTICLE INFO

Article history:
Received 19 October 2012
Received in revised form 13 March 2013
Accepted 17 March 2013
Available online 13 April 2013

Keywords:
Ocean color
Optically shallow water
Water clarity

ABSTRACT

Retrievals of water quality parameters from satellite measurements over optically shallow waters have been problematic due to bottom contamination of the signals. As a result, large errors are associated with derived water column properties. These deficiencies greatly reduce the ability to use satellites to assess the shallow water environments around coral reefs and seagrass beds. Here, a modified version of an existing algorithm is used to derive multispectral diffuse attenuation coefficient (K_d) from MODIS/Aqua measurements over optically shallow waters in the Florida Keys. Results were validated against concurrent *in situ* data ($K_d(488)$ from 0.02 to 0.20 m^{-1}, N = 22, R^2 = 0.68, Mean Ratio = 0.93, unbiased RMS = 31%), and showed significant improvement over current products when compared to the same *in situ* data (N = 13, R^2 = 0.37, Mean Ratio = 1.61, unbiased RMS = 50%). The modified algorithm was then applied to time series of MODIS/Aqua data over the Florida Keys (in particular, the Florida Keys Reef Tract), whereby spatial and temporal patterns of water clarity between 2002 and 2011 were elucidated. Climatologies, time series, anomaly images, and empirical orthogonal function analysis showed primarily nearshore–offshore gradients in water clarity and its variability, with peaks in both at the major channels draining Florida Bay. ANOVA revealed significant differences in $K_d(488)$ according to distance from shore and geographic region. Excluding the Dry Tortugas, which had the lowest climatological $K_d(488)$, water was clearest at the northern extent of the Reef Tract, and $K_d(488)$ significantly decreased sequentially for every region along the tract. Tests over other shallow-water tropical waters such as the Belize Barrier Reef also suggested general applicability of the algorithm. As water clarity and light availability on the ocean bottom are key environmental parameters in determining the health of shallow-water plants and animals, the validated new products provide unprecedented information for assessing and monitoring of coral reef and seagrass health, and could further assist ongoing regional zoning efforts.

1. Introduction

For several decades, satellite ocean color measurements have offered the ability to synoptically measure water quality parameters such as water clarity, turbidity, chlorophyll-*a* concentrations, and many others. Instruments such as the U.S. National Aeronautics and Space Administration's (NASA) Moderate Resolution Imaging Spectroradiometer (MODIS) onboard the satellites Aqua and Terra, and the associated algorithms developed by the ocean color community have provided a long time series of water quality data for many regions. Largely excluded from such analyses, however, have been optically shallow waters, defined here as regions where the benthos is visible from an above-water (or satellite-borne) sensor. In such environments, some of the satellite-derived remote sensing reflectance (R_{RS}, see Table 1 for description of symbols used in this paper) results from reflection of light off the benthos (Maritorena et al., 1994; Mobley & Sundman, 2003). When these bottom-contaminated R_{RS} are fed into current water quality or water clarity algorithms, large errors in derived products can occur. Specifically, bottom contamination has been shown to result in severe overestimation of chlorophyll concentrations (Cannizzaro & Carder, 2006; Carder et al., 2005; Hu, 2008; Schaeffer et al., 2011), particulate backscattering coefficients (b_{bp}; Carder et al., 2005), and diffuse attenuation coefficient for downwelling irradiance (K_d; Zhao et al., 2013).

The bottom contribution to satellite-measured signals is sometimes useful towards the derivation of K_d in optically shallow waters with high resolution sensors (*e.g.*, Landsat Thematic Mapper (TM), 30 m spatial resolution). One such method involves determining the exponential

* Corresponding author. Tel.: +1 727 553 3952.
E-mail address: bbarnes4@mail.usf.edu (B.B. Barnes).

0034-4257/$ – see front matter © 2013 Elsevier Inc. All rights reserved.
http://dx.doi.org/10.1016/j.rse.2013.03.016

Table 1
Description of symbols.

Symbol	Description	Units
K_d	Diffuse attenuation coefficient for downwelling irradiance	m^{-1}
E_d	Downwelling irradiance	W nm^{-1} m^{-2}
$E_d(0-)$	Subsurface downwelling irradiance	W nm^{-1} m^{-2}
L_w	Water-leaving radiance	W nm^{-1} m^{-2} sr^{-1}
R_{RS}	Remote sensing reflectance	sr^{-1}
r_{rs}	Subsurface remote sensing reflectance	sr^{-1}
a_t	Total absorption coefficient	m^{-1}
a_w	Absorption coefficient of pure water	m^{-1}
a_g	Absorption coefficient of gelbstoff	m^{-1}
a_{ph}	Absorption coefficient of phytoplankton pigments	m^{-1}
b_b	Total backscattering coefficient	m^{-1}
b_{bw}	Backscattering coefficient of pure water	m^{-1}
b_{bp}	Backscattering coefficient of suspended particles	m^{-1}
λ	Wavelength	nm
θ	Solar zenith angle	Degrees
z	Depth	m

decay slope of water leaving radiance (L_w) for regions in which pixels have varying depths but the same bottom albedo (Maritorena, 1996; Palandro et al., 2004). This procedure, however, is labor intensive and requires extensive prior knowledge of the environment, including high resolution raster bathymetry and benthic classification. Further, the required assumption that pixels used in these analyses are homogenous with exactly the same bottom albedo is often unrealistic in complex and spatially diverse systems such as coral reefs and seagrass beds. Finally, the repeat overpass frequency for sensors with the resolution required for such work (*e.g.*, 16 days for Landsat) is much less than that offered by ocean color satellites with lower spatial resolution (*e.g.*, 1–2 days for Aqua at 1 km resolution), and may thus miss much of the temporal variability in water clarity. As such, although deriving K_d from high resolution satellite data is sometimes feasible with intensive labor, it is operationally impractical for widespread implementation and analysis of spatiotemporal patterns in water clarity.

The nature of bottom contamination is such that within a region of optically shallow waters and homogenous albedo, the R_{RS} signal at geometrically shallow locations will be more affected than that at deeper locations, resulting in even larger errors in derived products. The correlation between depth and bottom-contaminated R_{RS} in such environments has been exploited in the creation of bathymetries from MODIS (Hu, 2008) and TM data (Lyzenga, 1981; Stumpf et al., 2003). Water clarity maps (derived from standard algorithms) of optically shallow waters, such as those around the Florida Reef Tract (FRT), show similar trends (Fig. 1). Fig. 1 shows MODIS-derived $K_d(488)$ using the Lee et al. (2005) algorithm, where changes in water clarity are clearly associated with bathymetry. This effect is also seen in the FRT region when MODIS data is processed using the default band-ratio algorithm for K_d (Mueller, 2000), further highlighting the need for an improved K_d algorithm for optically shallow waters.

Marine ecosystems located within optically shallow waters (*e.g.*, coral reefs, seagrasses and sponge beds) can be greatly affected by light availability, and thus water clarity. For example, as with all organisms performing photosynthesis, zooxanthellae (algae living in symbiosis within the coral tissues) require light for chemical energy creation. However, excess radiation (especially in the ultraviolet wavelengths) can cause oxidative stress in photosynthesizing marine organisms (Foyer et al., 1994; Jokiel, 1980) including corals (Fisk & Done, 1985; Hoegh-Guldberg & Jones, 1999; Lesser et al., 1990). Although corals and zooxanthellae have mechanisms to mitigate the effects of such stress (Ayoub et al., 2012; Shick & Dunlap, 2002; Shick et al., 1996), it can nevertheless deteriorate the symbiotic relationship between corals and algae, especially in conjunction with elevated sea temperatures. Under extreme stress, corals will expel the zooxanthellae from their tissues, resulting in a 'bleached' condition, often leading to mortality of the coral polyp (see reviews by Brown, 1997; Hoegh-Guldberg, 1999; Douglas, 2003, and others). The relationship between incident radiation and stress response in corals is also wavelength dependent (Lesser & Lewis, 1996; Zepp et al., 2008), highlighting the necessity for multispectral characterization of the light field reaching coral reefs. In a more general sense, decreases in water clarity are often associated with increased nutrient loading and subsequent increases in water column chlorophyll concentrations (Riley, 1956; Rodhe, 1948). Not only can this reduce light availability and thereby directly affect the health of both coral (*e.g.*, Abram et al., 2003) and seagrass (Moore & Wetzel, 2000) environments, but it can further reduce the competitive advantage of these ecosystem engineers (Hallock & Schlager, 1986; Hemminga, 1998).

In the absence of reliable satellite-derived water clarity data, *in situ* investigations of the relationship between light and optically shallow ecosystems must rely on localized water clarity monitoring and experimentation (*e.g.*, Fisk & Done, 1985; Gleason et al., 2006; Hoegh-Guldberg & Jones, 1999; Lesser et al., 1990; Moore & Wetzel,

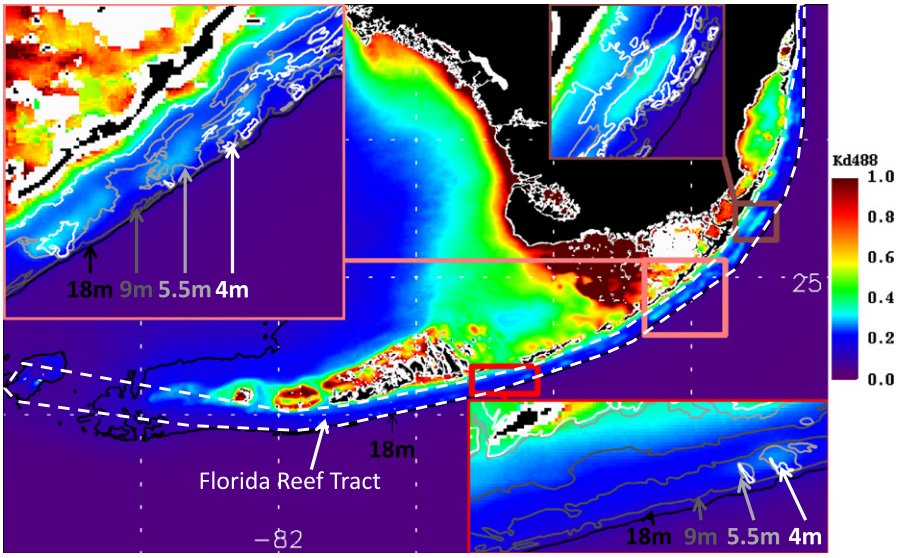

Fig. 1. February climatology of $K_d(488; m^{-1})$ calculated from standard K_d_Lee. Bathymetry contours overlaid are white = 4 m, light gray = 5.5 m, dark gray = 9 m, and black = 18 m. Approximate extent of Florida Reef Tract shown with white dashes. Land shown in black with white coastline. No data shown as white.

2000; Zepp et al., 2008). Even where long term monitoring programs exist, the extreme costs typically result in repeat sampling frequency and spatial distance between measurements large enough to potentially miss water clarity events and variations. In contrast, synoptic multispectral water clarity data from satellite measurements within optically shallow waters would allow regional assessment and monitoring of coastal nutrient loading mediation programs in near-real time. Further, such data would provide opportunities to continually assess light availability for coral reefs and seagrasses.

Given the known problems in existing satellite-based water clarity data products and the pressing need for such products to assess shallow marine ecosystems, the objective of this study was to develop a validated approach to derive water clarity parameters for optically shallow waters using MODIS data. Further, the use of these validated products in spatiotemporal pattern analysis, potential for implementation in regional management efforts, and the extension of the approach to other optically shallow waters are discussed.

2. Study Area — Florida Keys and the Florida Reef Tract

The Florida Keys are a limestone archipelago located at the southern tip of Florida (Fig. 2). These islands house over 73,000 residents (US Census Bureau, 2011) and are visited by approximately 2.5 million tourists each year who generate nearly 1.2 billion dollars for the region annually. Surrounding the Florida Keys is the Florida Keys National Marine Sanctuary (FKNMS), a 9600 km^2 management protected area created by the United States Congress in 1990 (Causey, 2002). Delineation of regions within the FKNMS is most commonly described according to water quality, the local circulation patterns and adjacent water masses (Klein & Orlando, 1994). Although waters within many of the FKNMS regions can be described as optically shallow at times, this work focuses solely on those waters south of the island chain. The Florida Reef Tract (FRT) is a 270 km arc of bank and patch reefs directly south and east of the Florida Keys. Coral cover within the FRT has precipitously declined over the last several decades (Andréfouët et al., 2002; Hughes, 1994; Palandro et al., 2001, 2008). These changes have been attributed to extreme temperature events (Jaap, 1985; Lirman et al., 2011; Warner et al., 1999), as well as changes in water quality (Hu et al., 2003; Lapointe et al., 2004) resulting from local anthropogenic activities (LaPointe & Clark, 1992) or exogenous sources such as Florida Bay (Smith, 1994) and Mississippi River (Hu et al., 2005; Ortner et al., 1995). Seagrass density in the region has also decreased, most often attributed to algal blooms and epiphyte buildup (LaPointe & Clark, 1992). Although chlorophyll blooms (Hu et al., 2003) and river plumes (Hu et al., 2005) can be quantified and tracked nearby coral reef and seagrass systems, errors in current algorithms due to bottom contamination prohibit quantitative satellite monitoring of the extent and fate of such events (or their impact on the benthos) as they enter optically shallow regions.

Easterly winds are typical for this region, setting up a westward current immediately south of the Lower Keys. These prevailing winds run perpendicular to the island chain in the Upper Keys, and thus do not largely contribute to nearshore currents. Instead, the proximity of the Florida Current (precursor to the Gulf Stream) to the Upper Keys leads to primarily northeastward currents in this subregion. Eddies resulting from the Florida Current also contribute to the westward flow in the Lower Keys. The Middle Keys are considered a transition zone between these two current regimes (Lee, 2012; Lee & Williams, 1999; Lee, T., et al., 2002). General circulation patterns also show large scale inundation of the FRT with Florida Bay waters occurring through a few channels between islands of the Florida Keys, especially Moser Channel, Long Key Channel, Channel #2 and Channel #5 (Smith, 1994; Porter et al., 1999; Lee & Smith, 2002; Lee, T., et al., 2002; Fig. 2). In fact, Fig. 2 appears to show increased attenuation in waters flowing into the FRT through the Middle Keys channels.

These general circulation patterns, coupled with the findings by LaPointe and Clark (1992) and Szmant and Forrester (1996) that the highest nutrient concentrations in the region were within the Middle Keys during summer months, lead to the widely held hypothesis that the Middle Keys region has the lowest water clarity. Boyer and Jones (2002) found the Marquesas region to have the highest chlorophyll concentrations, while several studies have found the Lower Keys to have clearest waters (Boyer & Jones, 2002; Klein & Orlando, 1994; Szmant & Forrester, 1996). Finally, strong gradients in water quality have been identified according to distance from shore, with offshore waters being the clearest and most oligotrophic (LaPointe & Clark, 1992; Szmant & Forrester, 1996).

The Florida Bay Water Quality Monitoring Program (see Boyer & Briceno, 2011) and the NOAA Atlantic Oceanographic and Meteorological Laboratory's South Florida Program (see Kelble & Boyer, 2007) are long term intensive monitoring efforts in the Florida Keys region designed to investigate spatiotemporal water quality patterns. These programs provide a long term series of nutrient dynamics snapshots in the region, but are lacking in temporal resolution (>2 months) and are not spatially synoptic. Regional managers are currently planning a rezoning of specific protection areas within the FKNMS (NOAA, 2007, 2012). Synoptic water clarity information, as well as investigations of the effects of light on benthic communities, would be a timely and valuable addition to the dataset informing this process.

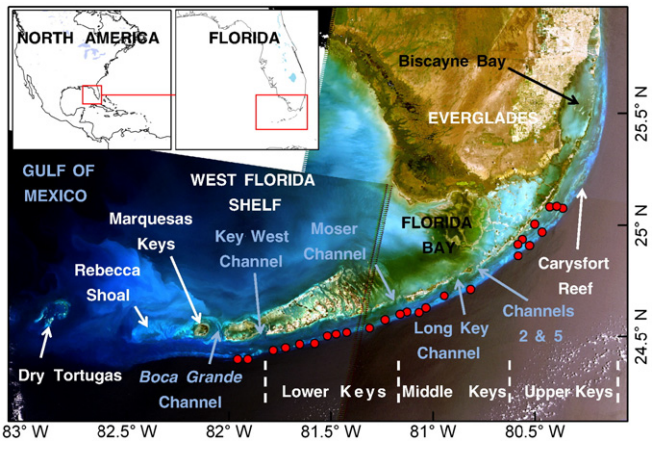

Fig. 2. Map showing sampling locations (red circles) and regions discussed in this paper, overlaid on composite of three Landsat5 TM true color images from 29 March 2008 (Lower Keys) and 23 April 2008 (Upper Keys and Everglades).

3. Satellite derived attenuation in optically shallow waters

3.1. Algorithm development

Among the current algorithms to derive K_d from MODIS data, Zhao et al. (2013) found that the Lee et al. (2005) algorithm (hereafter termed 'standard K_d_Lee') performed better than other empirical methods when validated against concurrent *in situ* data from south Florida and Caribbean waters. Nevertheless, the algorithm was designed for optically deep waters, thus generally limited in its applicability for measurements contaminated by bottom reflectance. This algorithm uses a simple function to derive multispectral K_d:

$$K_d = (1 + 0.005\theta)a_t + m_1(1 - m_2 e^{m_3 a_t})b_b, \quad (1)$$

where a_t is the total absorption coefficient, b_b is the total backscattering coefficient, θ is the sun zenith angle in air, and m_1, m_2, and m_3 are constants of 4.18, 0.52, and −10.8, respectively. The inherent optical properties (IOPs; a_t and b_b) and K_d are wavelength (λ) dependent, but wavelength notation has been omitted for simplicity. IOPs are derived using the most recent version of the Quasi-Analytic Algorithm (QAAv5;

hereafter termed 'QAA') developed by Lee., Z., et al. (2002, 2009). This process starts with the estimation of a_t at a reference wavelength (ref), typically 555 nm for SeaWiFS and 547 nm for MODIS:

$$a_t(\mathrm{ref}) = a_w(\mathrm{ref}) + 10^{-1.146-1.366\chi-0.469\chi^2}, \quad (2)$$

where a_w is the pure water absorption coefficient from Pope and Fry (1997) and:

$$\chi = \log\left(\frac{r_{rs}(443)+r_{rs}(490)}{r_{rs}(\mathrm{ref})+5\frac{r_{rs}(667)}{r_{rs}(490)}r_{rs}(667)}\right), \quad (3)$$

where r_{rs} is the underwater remote sensing reflectance, $r_{rs} = [R_{RS} / (0.52 + 1.7 * R_{RS})]$. This a_t is then used to retrieve b_{bp} at the reference wavelength:

$$b_{bp}(\mathrm{ref}) = \frac{u(\mathrm{ref}) * a_t(\mathrm{ref})}{1-u(\mathrm{ref})} - b_{bw}(\mathrm{ref}), \quad (4)$$

where b_{bw} is the pure water backscattering coefficient from Morel (1974), and $u = [b_b / (a_t + b_b)]$ as calculated from r_{rs}:

$$u(\lambda) = \frac{-g_0 + \left[(g_0)^2 + 4g_1 r_{rs}(\lambda)\right]^{1/2}}{2g_1}, \quad (5)$$

with coefficients g_0 and g_1 equal to 0.089 and 0.125, respectively. The value of b_{bp} at the reference wavelength is subsequently used to derive multispectral b_b (Gordon & Morel, 1983; Smith & Baker, 1981) and a_t:

$$b_b(\lambda) = b_{bp}(\mathrm{ref})\left(\frac{\mathrm{ref}}{\lambda}\right)^Y + b_{bw}(\lambda), \quad (6)$$

$$a_t(\lambda) = \frac{[1-u(\lambda)][b_b(\lambda)]}{u(\lambda)}, \quad (7)$$

with

$$Y = 2.0\left(1-1.2e^{\left(-0.9\frac{r_{rs}(443)}{r_{rs}(547)}\right)}\right). \quad (8)$$

Using hyperspectral R_{RS} data of optically shallow waters, Zhao et al. (2013) also found that K_d calculated with this process showed a large effect of bottom contamination. Since the QAA begins with estimation of a_t at a reference wavelength, any errors in this single step (Eq. 2) would be propagated throughout the QAA and into the derivation of K_d. The reference wavelength of 555 nm for SeaWiFS was originally chosen because $a_t(555)$ is relatively stable in oceanic waters where at the same time satellite measured R_{RS} maintains high fidelity compared to those at longer wavelengths (*e.g.*, 670 nm), but longer wavelengths were proposed for nearshore or river plume environments (Lee, Z., et al., 2002) where higher chlorophyll or sediment concentrations cause large variations in $a_t(555)$. Variable bottom contamination will also cause large changes in the measured R_{RS} (and subsequently derived a_t), especially at shorter wavelengths. At longer wavelengths, since the attenuation coefficient due to water molecules (a_w) is much higher, less bottom contamination in the measured R_{RS} is expected. Indeed, citing the wavelength-dependent impacts of bottom contamination, Carder et al. (2005) found improvements in satellite-derived b_{bp} and chlorophyll-*a* concentration measurements using 670 nm (as opposed to 555 nm for SeaWiFS) in extant ratio-based algorithms for optically shallow waters in this region with depths as shallow as 2 m. For optically shallow waters deeper than 5 m, errors in these same parameters were reduced by two to three fold (Carder et al., 2005). As such, for this research we modified the QAA to use 667 nm as a reference wavelength.

To apply the QAA with 667 nm as the reference wavelength, the formula for $a_t(\mathrm{ref})$ was modified from Eq. (18) in Lee, Z., et al. (2002) to:

$$a_t(\mathrm{ref}) = a_w(\mathrm{ref}) + 0.07\left(\frac{r_{rs}(\mathrm{ref})}{r_{rs}(443)}\right)^{1.1}, \quad (9)$$

and used in place of Eqs. (2) and (3). Eqs. (4)–(8) were applied as above. The multispectral a_t and b_b were subsequently input into Eq. (1) to calculate 'modified' K_d_Lee.

The theoretical background for this algorithm modification is nullified for waters shallow and clear enough that bottom contamination has an effect on the $R_{RS}(667)$. Even though Carder et al. (2005) showed potential improvements in water property derivations in optically shallow waters down to 2 m depth by using longer wavelengths as a reference, within that work a 5 m depth threshold was selected to minimize errors throughout the application depth range. Accordingly, the scope of data considered in this analysis is limited to waters with bottom depths deeper than 5 m. Schaeffer et al. (2011) found bottom reflectance affects satellite chlorophyll retrievals in coastal Florida waters shallower than 25 m. As such, for the purposes of this research, thresholds of 5 m and 30 m are used to delineate the shallow and deep extent of optically shallow waters within the Florida Keys ecosystem.

3.2. Sensitivity simulations

A mathematical simulation was performed to investigate differences in performance of the standard and modified K_d_Lee algorithms. First, typical ranges of $a_{ph}(440)$, $a_g(440)$ and $b_{bp}(440)$ in the FRT region were defined from field data collected during this study. A continuous range of 0–50% of benthic albedo (at 550 nm) was used to simulate conditions for a range of benthic environments in the Florida Keys, with corals (often less than 5% albedo at 550 nm) and carbonate sand (up to and exceeding 50% albedo at 550 nm) being end members (Hochberg et al., 2003; Werdell & Roesler, 2003). Using the semi-analytical model described by Lee et al. (1999), various combinations of IOPs, bottom depths, and benthic albedos were used to simulate hyperspectral R_{RS} spectra. The input IOPs were also used to calculate the 'true' K_d, by means of Eq. (1). The R_{RS} was then fed into the QAA_v5 and the modified QAA (and subsequently K_d_Lee) to derive standard and modified K_d_Lee. Error of these algorithms was then calculated as [(simulated_K_d − truth)/truth].

3.3. Satellite data

All MODIS Aqua (MODIS/A, 2002–2011) Level 0 data for the Florida Keys region were downloaded from the NASA Goddard Space Flight Center ocean color website (http://oceancolor.gsfc.nasa.gov), a total of 2281 satellite passes. The data were processed at 250 m resolution using SeaDAS (version 6.2) software and default processing parameters (Baith et al., 2001). The 645 nm band had a nominal ground resolution of 250 m while other bands at 500- and 1000-m resolutions were interpolated to 250 m. For each pass, using the standard algorithms implemented in SeaDAS, Level 2 data were created including R_{RS} and standard K_d_Lee for the MODIS bands centered at 412, 443, 469, 488, 531, 547, 555, 645, 667, and 678 nm. These products were masked using the Level 2 flags ATMFAIL, LAND, HILT, and CLDICE (see Patt et al., 2003), then subsequently mapped to an equidistant cylindrical projection with bounds 24 to 26 N, 83 to 80 W. Hereafter, the term 'pixel' refers to a 250 m × 250 m data bin, which has a set latitude and longitude in this projected data frame and a spatial area of 62,500 m^2. All data were stored in Hierarchical Data Format 4 (HDF4) computer files.

Computer programs were implemented to apply the QAA with 667 nm as a reference wavelength (Eqs. 4–9) to the above processed MODIS/A R_{RS} data. Using Eq. (1), a_t and b_b from the modified QAA were used to derive modified K_d_Lee for each band. As with the above standard-processed data, multispectral K_d data were stored in HDF4 files. Unless otherwise stated, all data manipulation and processing were conducted using IDL version 8.0 (Interactive Data Language; Exelis Visual Information Solutions). For quality control during validation, extracted pixels were excluded if they were adjacent to a masked pixel (*i.e.*, if any of the 9 pixels within a 3 × 3 pixel box with the pixel of interest at the center had been masked). Extracted pixels were also removed from validation analysis if the standard deviation of the values from this 3 × 3 box was greater than 10% of the mean. These two quality control procedures are hereafter termed 'spatial homogeneity test,' and were performed on each algorithm and band independently. These quality control measures were not applied during composition of climatologies and multi-year time series. Instead, additional Level 2 quality control flags were used to discard low-quality data: HIGLINT, HISATZEN, STRAYLIGHT, COCCOLITH, HISOLZEN, LOWLW, CHLFAIL, NAVWARN, MAXAERITER, CHLWARN, ATMWARN, NAVFAIL, and FILTER (for description of quality control flags, see Patt et al., 2003).

For synoptic visualization of algorithm performance, the entire time series of MODIS/A data were used to calculate the average and standard deviation of these data within specific time intervals. Monthly means were calculated as the average value at each pixel for an individual month and year. Monthly climatologies are the mean of all data for a particular month, regardless of the year. Monthly anomalies (monthly mean minus the corresponding monthly climatology), monthly standard deviation and monthly coefficient of variation were also calculated for each month in the MODIS/A time series. Pixels masked in the data processing were treated as empty values and thus did not affect the mean and standard deviation calculations. Finally, percent difference in methods was calculated using monthly climatologies as [(standard − modified) / modified].

3.4. In situ data collection and processing

Field data for validation of these satellite products was collected from April 8–22, 2011 and July 31–August 22, 2012. Twenty-six stations spaced throughout the shallow waters south of Florida Keys were each visited at least 4 times, but up to 7 times, for a total of 145 sampling events (Fig. 2). All data were collected within 2 h of the local solar noon. At each sampling, a free-falling hyperspectral profiler (HyperPRO, Satlantic, Halifax, NS, Canada) optical remote sensing system provided in-water hyperspectral (400–735 nm, interpolated every 1 nm) measures of downwelling irradiance [$E_d(z,\lambda)$], upwelling radiance [$L_u(z,\lambda)$], and depth. The instrument was allowed to drift approximately 5 to 10 m away from the boat to avoid shading interference, and three profiles were conducted at each sampling. Pressure tare was completed on deck prior to each instrument deployment. HyperPRO data were quality controlled by excluding data with a tilt and roll > 5°.

Wave focusing of incident light contaminated the measured $E_d(z)$, resulting in large deviations from the expected log-linear nature of E_d with depth. As such, for each cast, $E_d(z,\lambda)$ were binned (averaged) to 0.3 m depth intervals, then natural logarithm transformed and plotted against measurement depth. These graphs were manually processed to locate the longest sequence of data showing approximately linear decay. Data from this portion of the profile was used to calculate [$K_d(\lambda)$] from a linear regression of $\ln[E_d(z,\lambda)/E_d(0-,\lambda)]$ and depth. Further, HyperPRO data were only considered reliable if the difference in K_d from any two (of the three) replicate profiles was less than 0.01 m^{-1} (typically ~10% difference), in which case the average K_d of these two replicates was determined for use in validation. In total, seventy-six hyperspectral K_d *in situ* measurements fit this qualification and were used for satellite algorithm validation.

3.5. Algorithm validation methods

Concurrent (same day and location) satellite and *in situ* data were compared statistically using coefficients of determination (R^2), linear regression, root mean squared (RMS) percentage difference, mean ratio and standard deviation ratio. Due to error in both satellite and *in situ* datasets, RMS was performed on an unbiased percent difference [(satellite − *in situ*) / (0.5 ∗ satellite + 0.5 ∗ *in situ*)], hereafter termed 'URMS' and reported as a percentage (Hooker et al., 2002). The significance level (α) for all statistical tests was 0.05.

3.6. Algorithm validation results

It is important to reiterate that this algorithm and all quality control procedures were developed prior to the validation shown here, and that no *in situ* data were used for algorithm tuning or calibration. There were 13 concurrent $K_d(488)$ matchups between the standard K_d_Lee satellite product and *in situ* data (Fig. 3; range 0.02–0.20 m^{-1}). These data showed a weak, yet significant, positive relationship ($R^2 = 0.37$, linear regression slope = 0.68 and intercept = 0.10, p-value = 0.03). Ratio statistics indicate that satellite derived $K_d(488)$ for these data is 1.61 times the measured $K_d(488)$ with a standard deviation ratio of 0.65 and URMS error of 50%. For comparison, the modified K_d_Lee(488) algorithm produced 22 pixels with concurrent *in situ* measurements of the same range (Fig. 3). The different numbers of matchups between the two satellite algorithms result from higher spatial heterogeneity in the standard K_d_Lee product, which caused more data to be discarded through the 3 × 3 spatial homogeneity test. These matchups showed a much stronger positive relationship ($R^2 = 0.68$, slope = 0.95, intercept = −0.002, p-value < 0.0001), with K_d(satellite) = 0.93 ∗ K_d(*in situ*), and a standard deviation ratio of 0.27. URMS was reduced from 50% to 31%.

Table 2 summarizes the matchup statistics for all bands of K_d. Due to the spatial homogeneity test of the satellite data, the number of matchups was not constant across all wavelengths, or between the standard and modified algorithms (matchups were especially reduced for the standard K_d_Lee, which was much more spatially heterogeneous than the modified K_d_Lee). To ensure a fair comparison, only *in situ* data which had matching satellite data from both methods ('common') were included in the first two panels of Table 2. The third panel includes all modified K_d_Lee matchups.

Most indices showed improved statistical relationships between satellite and *in situ* data when using the modified K_d_Lee in place of the standard K_d_Lee. For wavelengths shorter than 500 nm, K_d matchups showed improvements *via* increased R^2, linear regression slope closer to one and intercept closer to zero, smaller p-value, mean ratio closer to one, smaller standard deviation ratio, and smaller URMS (Table 2). For wavelengths above 600 nm, improvements in R^2 and the linear regression are not always apparent, but are seen in the mean ratio, standard deviation ratio, and URMS. Statistical measures for the remaining wavelengths (531, 547, and 555 nm) show mixed measures of performance between the standard and modified K_d_Lee. Despite improvements in the linear regression statistics, R^2 and URMS were generally not improved by the modified K_d_Lee at these wavelengths.

3.7. Discussion of validation results

As demonstrated in Fig. 1, co-occurring variations in bottom depth and satellite-derived water parameters may indicate bottom contamination. The main sources of nutrients into the FRT region are the Florida Keys themselves and the channels between islands carrying Florida Bay water (Lapointe & Clark, 1992). Higher K_d values are expected nearest these nutrient sources or in contiguous plumes extending from them. Monthly climatologies of $K_d(488)$ derived using the standard K_d_Lee algorithm, however, show a different pattern (see Fig. 1 showing February climatology as an example). Overlaid with

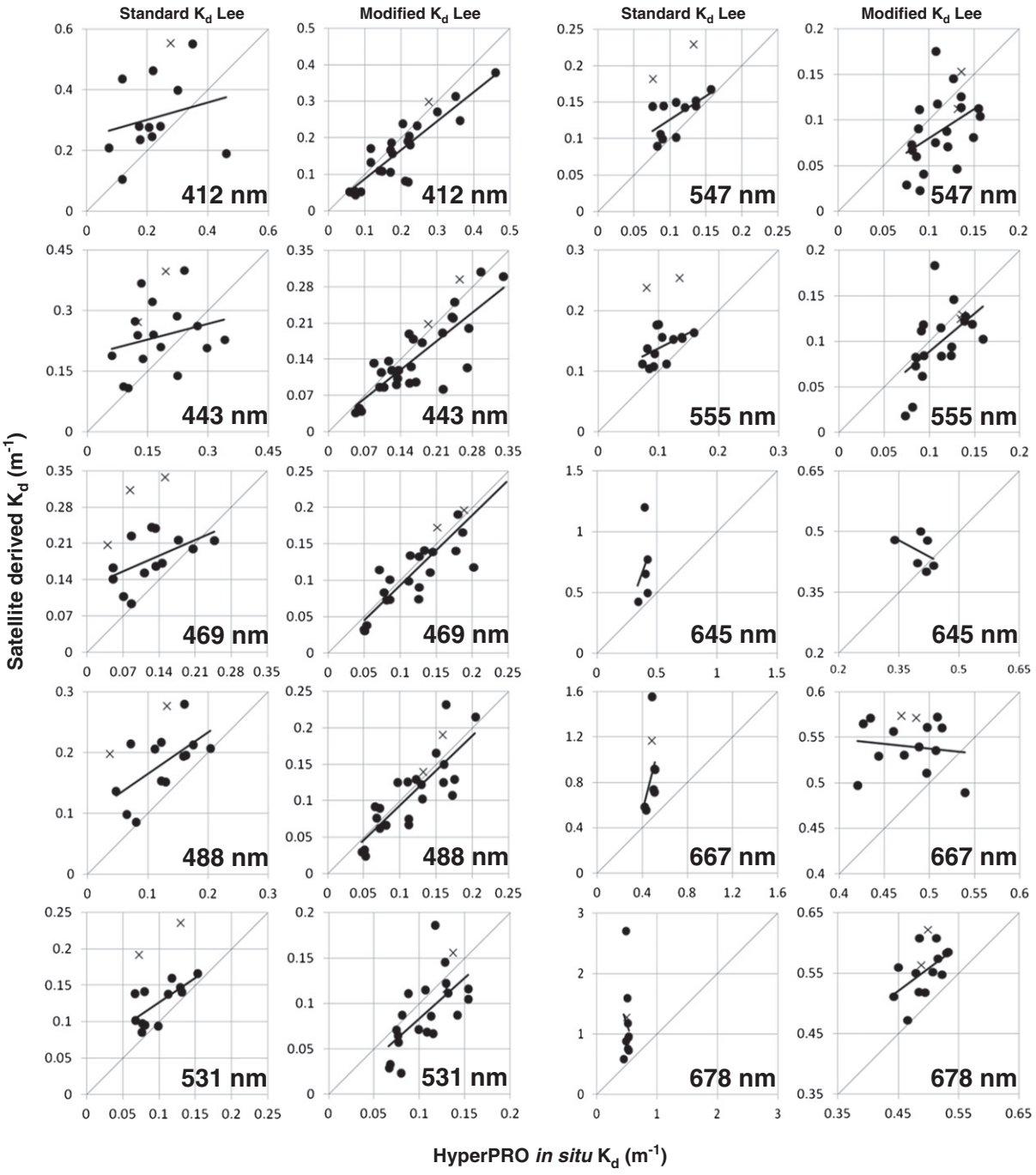

Fig. 3. Comparison between satellite and *in situ* K_d data. Columns 1 and 3 show K_d from the standard K_d_Lee, while columns 2 and 4 were derived using the modified K_d_Lee. Circles show data from stations deeper than 5 m, while matchups < 5 m are marked by '×'. Linear regression line (dark black) shown for <5 m matchups only. Gray diagonal is 1:1 reference.

bathymetric contour lines, increases in $K_d(488)$ tend to co-occur with bottom depth even away from the land. Such visualizations reiterate the problem with current algorithms, *i.e.* modeled parameters vary with bottom depth, and thus represent the intensity of bottom contribution to the R_{RS} signal and subsequent contamination in the derived water quality parameters.

In contrast, the exact same R_{RS} data were used in the creation of Fig. 4, instead processed using the modified K_d_Lee algorithm. With the exception of data within the 4 m contour line, the main variation in water clarity appears to be along an onshore–offshore gradient, regardless of water depth. This visualization expands the argument of improvement in water clarity derivations using the modified K_d_Lee(488) beyond that offered by the limited number of matchups with *in situ* data. However, such maps also clearly show the failure of the modified K_d_Lee(488) at very shallow (less than ~5 m) depths (especially see Carysfort Reef area, top right inset in Fig. 4), where the modified K_d_Lee(488) may even show larger errors than the standard K_d_Lee(488). Further, these maps must be viewed with caution — although they show $K_d(488)$ derived for all pixels in the scene, the algorithm has only been validated for bottoms deeper than 5 m. Focusing only on such waters (5–30 m depth), percent difference calculations show that the standard K_d_Lee algorithm overestimates the true $K_d(488)$ by a factor of 2 throughout much

Table 2
Summary of statistics for concurrent satellite and *in situ* measurements of multispectral K_d.

	Band	Range	N	R^2	Slope	Intercept	p-Value	Mean ratio	STDEV ratio	URMS (%)
Standard K_d_Lee (common)	K_d(412)	0.07–0.46	11	0.06	0.28	0.25	0.48	1.68	0.94	0.62
	K_d(443)	0.06–0.34	15	0.06	0.26	0.19	0.37	1.54	0.77	0.55
	K_d(469)	0.05–0.25	12	0.31	0.42	0.12	0.06	1.67	0.79	0.55
	K_d(488)	0.05–0.20	12	0.39	0.68	0.09	0.03	1.60	0.68	0.50
	K_d(531)	0.07–0.15	12	0.47	0.68	0.06	0.01	1.32	0.33	0.32
	K_d(547)	0.08–0.16	11	0.41	0.64	0.06	0.03	1.25	0.28	0.28
	K_d(555)	0.07–0.16	11	0.57	0.61	0.07	0.01	1.27	0.23	0.28
	K_d(645)	0.34–0.42	5	0.09	2.78	−0.39	0.62	1.79	0.75	0.58
	K_d(667)	0.42–0.51	7	0.18	3.85	−1.00	0.34	1.76	0.66	0.56
	K_d(678)	0.45–0.53	9	0.02	−3.27	2.80	0.73	2.29	1.36	0.74
Modified K_d_Lee (common)	K_d(412)	0.07–0.46	11	0.92	0.76	0.04	<0.01	1.00	0.20	0.18
	K_d(443)	0.06–0.34	15	0.74	0.80	0.01	<0.01	0.89	0.25	0.31
	K_d(469)	0.05–0.25	12	0.85	1.10	−0.01	<0.01	0.97	0.29	0.28
	K_d(488)	0.05–0.20	12	0.70	0.98	0.00	<0.01	0.98	0.27	0.26
	K_d(531)	0.07–0.15	12	0.52	1.15	−0.03	0.01	0.79	0.34	0.49
	K_d(547)	0.08–0.16	11	0.34	0.97	−0.02	0.06	0.79	0.36	0.53
	K_d(555)	0.07–0.16	11	0.29	0.89	−0.01	0.09	0.83	0.41	0.55
	K_d(645)	0.34–0.42	5	0.09	−0.38	0.61	0.63	1.16	0.17	0.19
	K_d(667)	0.42–0.51	7	0.23	0.34	0.39	0.28	1.14	0.08	0.15
	K_d(678)	0.45–0.53	9	0.07	0.28	0.43	0.51	1.13	0.07	0.14
Modified K_d_Lee (all)	K_d(412)	0.05–0.46	24	0.78	0.79	0.01	<0.01	0.84	0.24	0.36
	K_d(443)	0.05–0.34	28	0.70	0.79	0.01	<0.01	0.86	0.24	0.34
	K_d(469)	0.04–0.25	22	0.75	0.96	0.00	<0.01	0.93	0.26	0.28
	K_d(488)	0.02–0.20	22	0.68	0.95	0.00	<0.01	0.93	0.27	0.31
	K_d(531)	0.03–0.16	20	0.40	0.90	−0.01	<0.01	0.83	0.31	0.44
	K_d(547)	0.03–0.16	20	0.18	0.64	0.02	0.06	0.78	0.33	0.52
	K_d(555)	0.03–0.17	18	0.28	0.83	0.01	0.02	0.88	0.34	0.45
	K_d(645)	0.34–0.45	6	0.19	−0.53	0.66	0.39	1.13	0.18	0.18
	K_d(667)	0.42–0.55	13	0.02	−0.10	0.59	0.66	1.14	0.11	0.16
	K_d(678)	0.38–0.57	13	0.30	0.74	0.19	0.05	1.12	0.07	0.13

Range shows spread of *in situ* measurements, N = number of matchups, R^2 = coefficient of determination, URMS = unbiased root mean squared percent difference (see Section 3.4 for details), 'common' indicates *in situ* measurements with quality controlled satellite K_d from both algorithms.

of the FRT, and especially in spring and summer (Fig. 5 right column). This is especially true for the Upper Keys and Rebecca Shoal regions, where three- to four-fold errors in standard K_d_Lee retrievals are common.

Application of the modified K_d_Lee algorithm, however, does affect K_d retrievals for waters outside the FRT (Fig. 5). In the percent difference images, this is especially prevalent for the West Florida Shelf (WFS) and north of the Lower Keys islands during spring and summer months, but also can be seen in the extremely clear and deep waters of the Florida Straits (Fig. 5 right column). The difference in K_d(488) retrievals from the two algorithms for these regions is typically less than ±50% (compared to 100–>400% within the FRT). As the water is extremely clear when and where these differences outside the FRT occur, the discrepancy in K_d(488) between the two satellite algorithms in these instances is typically <0.02 m^{-1}. For comparison, within the FRT region, this difference typically ranges from 0.06 to 0.12 m^{-1}. Many coastal regions of mainland Florida, including Biscayne and

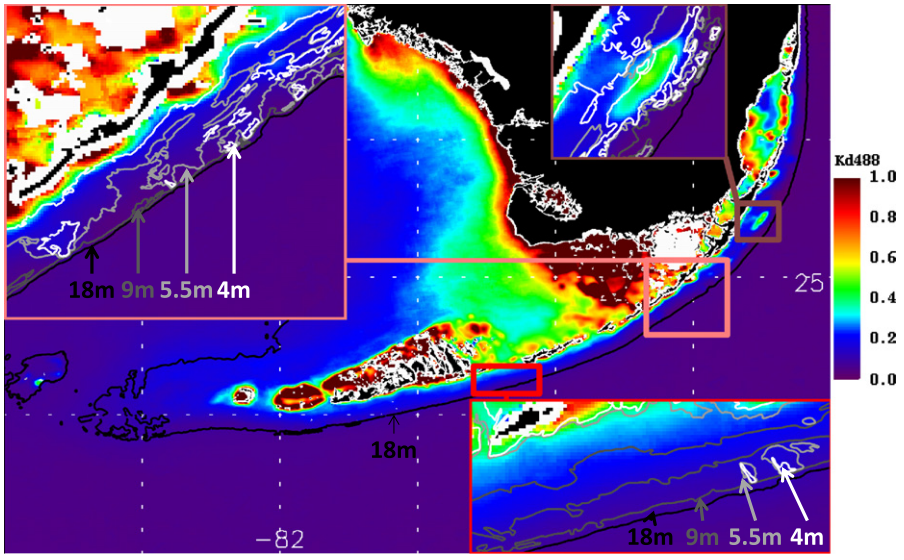

Fig. 4. February climatology of K_d(488; m^{-1}) calculated from modified K_d_Lee. Bathymetry contours overlaid are white = 4 m, light gray = 5.5 m, dark gray = 9 m, and black = 18 m. Land shown in black with a white coastline. No data shown as white. Note that compared with Fig. 1, the correlation between K_d and bathymetry has been significantly reduced.

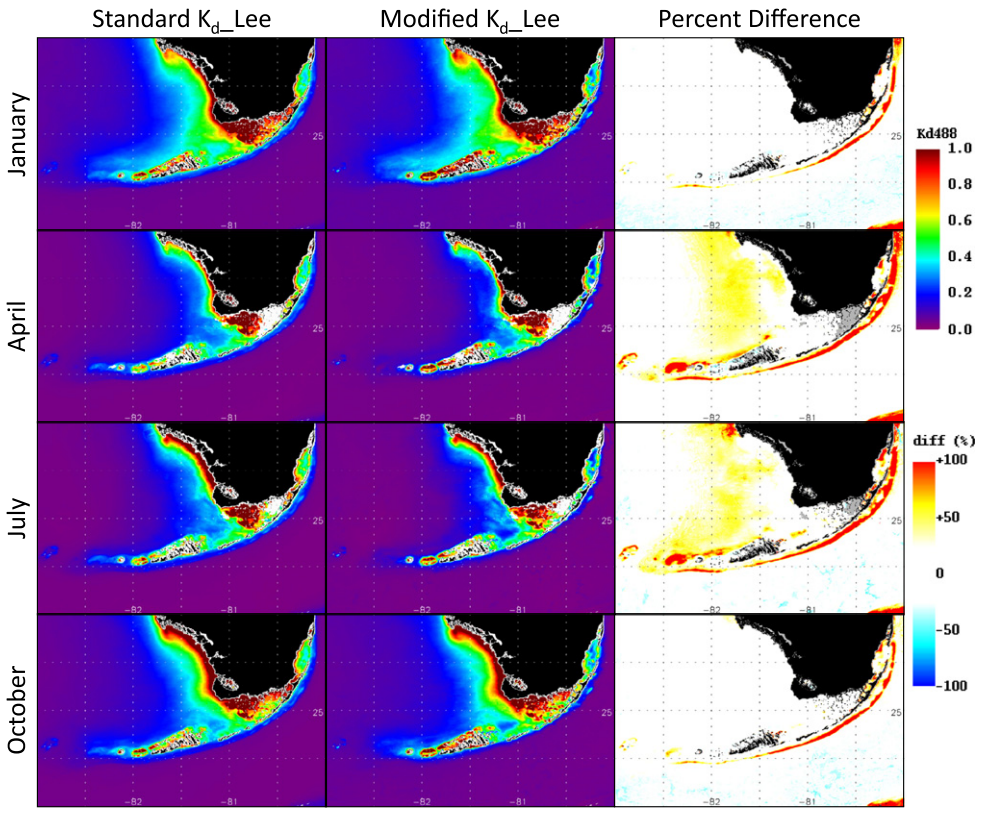

Fig. 5. Monthly climatologies of $K_d(488; m^{-1})$ derived using standard (left column) and modified K_d_Lee (middle column). Land shown in black with a white coastline. No data shown as white. Percent difference between these images shown in the right column with no data shown as gray.

Florida Bays, also show large (up to 0.1 m^{-1}) differences between the two algorithms, which are not seen in the percent difference images due to the overall high $K_d(488)$ values in these regions.

The modified algorithm did not improve K_d retrievals equally for all wavelengths. The most prominent improvements were seen in the shorter (<500 nm) wavelengths, but results were mixed for other wavebands. For longer wavelengths (>600 nm), there was little difference between the R^2 and linear regression statistics for the standard and modified algorithms. However, coupling the other statistical indices (mean ratio, standard deviation ratio and URMS) with the graphical representation of matchups shows that the modified algorithm calculates K_d closer to the *in situ* values than does the standard K_d_Lee. Nevertheless, the modified K_d_Lee cannot resolve the variation in these data points because within such clear waters, K_d in these longer wavelengths is dominated by the constant water absorption coefficient. Lastly, neither the standard nor modified K_d_Lee showed marked improvement over the other in the green wavelengths (531, 547, and 555 nm). This is partially due to the exclusion of MODIS/A data for spatial heterogeneity, which occurred more frequently for the standard than the modified K_d_Lee. Indeed, restricting the statistical analyses to the matchups used in the standard algorithm validation yields greatly improved performance from the modified method.

The sensitivity simulation was used to investigate the relative performance of the two algorithms without *in situ* measurement error or differences in numbers of validation points. The results from this simulation (Fig. 6) indicate that the modified K_d_Lee tends to slightly underestimate the true K_d in most normal FRT waters, while the opposite is seen for the standard K_d_Lee. In the blue and green wavelengths and deeper waters (>10 m), the magnitude of the error is approximately equal for these two algorithms. Shallower depths (<10 m), however, show much larger errors in the standard K_d_Lee at all wavelengths, clearly a result from bottom reflectance (perceived as higher b_{bp} and a_t throughout the standard QAA algorithm). The underestimation by the modified K_d_Lee, on the other hand, was an expected result of bottom contribution in the shorter wavelengths. This is due to the fact that even if water properties at the reference wavelength are stable, measured R_{RS} in the shorter wavelengths has been impacted by benthic contributions. As a result, although $a_t(\text{ref})$ and $b_{bp}(\text{ref})$ are reasonably estimated, lower $a_t(\lambda)$ (Eq. 7) would be resulted from an elevated $u(\lambda)$ (Eq. 5) where the R_{RS} have extra contributions from the benthos. Lower $a_t(\lambda)$ will subsequently result in an underestimation of K_d for shorter wavelengths (Eq. 1). Despite this underestimation, the bias of the modified K_d_Lee is relatively stable with increasing benthic albedo compared to the standard K_d_Lee, especially at shallower depths. It is important to note that although a range of benthic albedo values from 0 to 50% is shown in Fig. 6, the spatial heterogeneity of benthic environments in the FRT (and other coral reef systems) means that it is unlikely that either of these extremes in benthic albedo would be reached for a 250 m × 250 m pixel. Finally, simulated standard K_d_Lee in the red wavelengths showed extremely large errors with increasing benthic albedo, while the modified K_d_Lee showed almost no errors. Overall, this simulation highlighted the failures of the standard K_d_Lee in response to bottom contamination, while demonstrating improved performance of the modified K_d_Lee, especially in very shallow waters and in the red wavelengths.

3.8. Application considerations

The modified algorithm described here can be used to derive the diffuse attenuation coefficient in clear shallow waters (>5 m depth), and shows substantial improvement over the standard K_d_Lee in several wavelengths. Implementation of this algorithm requires R_{RS} data at

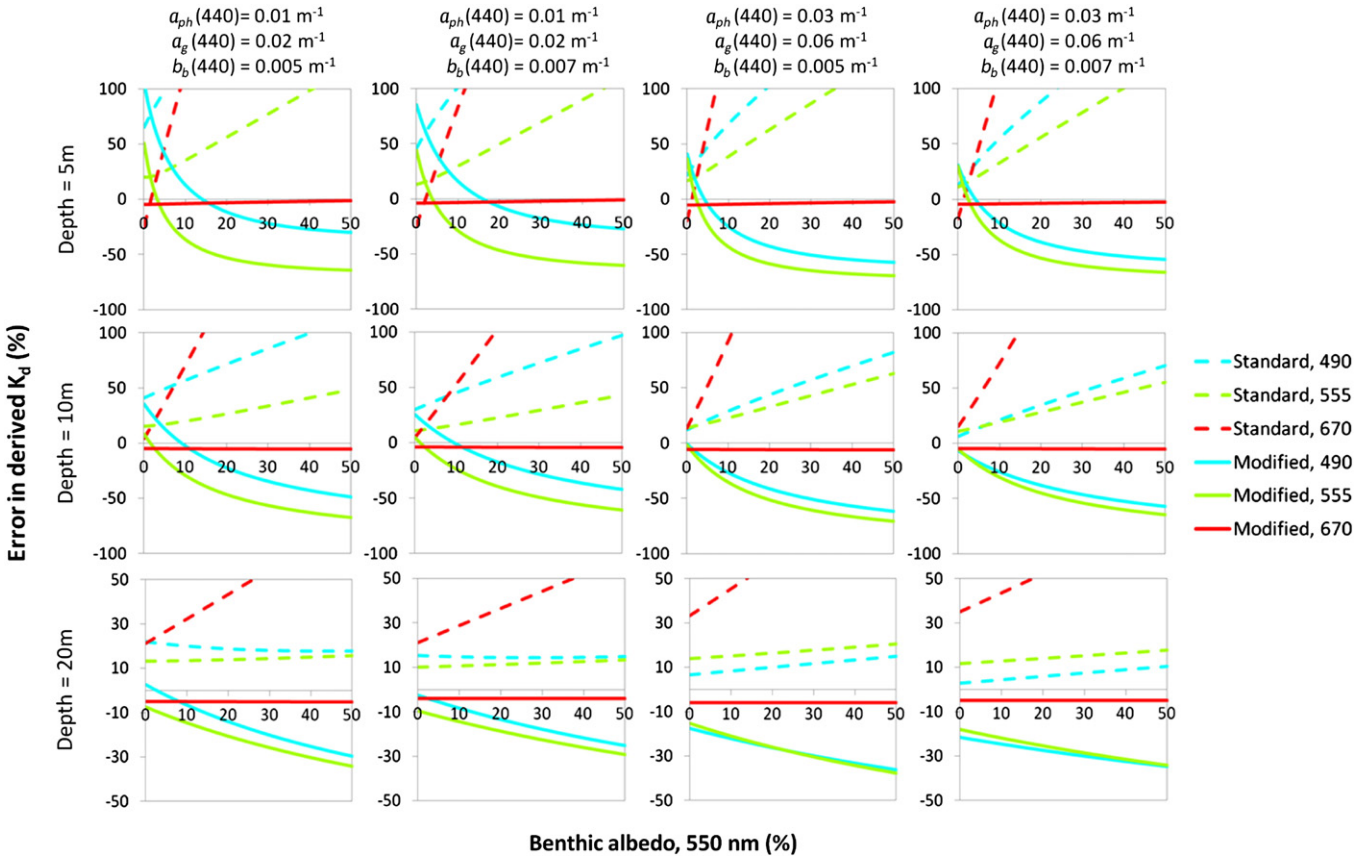

Fig. 6. Simulated percent error of standard (dashed) and modified (solid) K_d_Lee at 490 (blue), 555 (green), and 670 nm (red) for typical FRT waters.

only three bands (centered at 443, 547, and 667 nm for MODIS), which can then be applied to any other visible band (*e.g.*, 488). These, or similar, bands are within the ongoing data streams from the MODIS instruments on both Aqua and Terra, as well as in the historical Coastal Zone Color Scanner (CZCS), Sea-Viewing Wide Field of View Sensor (SeaWiFS, 1997–2010), and Medium Resolution Imaging Spectrometer (MERIS, 2002–2012) datasets. Further, this algorithm lends itself to application using data from the Visible Infrared Imaging Radiometer Suite (VIIRS, 2011–present) instrument for ongoing and future assessment of water clarity in optically shallow environments. Finally, as *in situ* measurements of K_d in optically shallow waters may have large errors due to wave-focusing throughout the water column, this technique may also be applied to shipborne R_{rs} measurements. Concurrent with E_d profiles, such application would provide independent verification of the E_d-derived K_d.

The validation dataset was collected in optically shallow waters south and east of the Florida Keys (5–30 m depth), and showed large differences in K_d(488) retrievals between the standard and modified algorithms. Outside this FRT region, with some exceptions (notably, WFS in spring and nearshore mainland Florida), there is widespread agreement between the standard and modified K_d_Lee. Since the standard K_d_Lee algorithm has been validated in this region (Zhao et al., 2013), such agreement indicates increased applicability of the modified algorithm, both outside the FRT (spatially) and beyond the range of its validation dataset. Similarly, due to the local validation of the standard K_d_Lee, exceptions to this agreement indicate bounds for the potential applicability of the modified algorithm. Specifically, K_d retrievals from the modified algorithm for extremely shallow and highly attenuating waters (Biscayne and Florida Bays, as well as nearshore mainland Florida) are likely erroneously overestimated. For other regions of disagreement, such as the WFS in spring, we find that the scale of the difference is not sufficient to justify a switch to the standard K_d_Lee.

Although not directly tested against *in situ* data from other regions, we feel that the modified K_d_Lee would yield similar improvements in water clarity retrievals for other optically shallow environments. To illustrate this potential applicability, a MODIS/A pass including the Belize Barrier Reef region was processed using the standard and modified K_d_Lee (Fig. 7). Although no bathymetric data were available for this region, pixels which showed high K_d(488) derived using the standard K_d_Lee appear to co-occur with areas where the bottom is clearly visible in the true color image. Using the modified algorithm, many of these apparently artificially elevated K_d measurements do not appear to be influenced by bottom contamination. However, as seen in the FRT (Carysfort reef area, Figs. 4 & 5), even larger errors in K_d products are seen for extremely shallow regions using the modified algorithm. Nevertheless, given the extremely large bottom reflectance signal compared to water column reflectance for shallow (>5 m) clear waters, accurate water property retrievals at these locations from ocean color data still requires further research, for example by explicitly taking into account both bottom depth and albedo in the algorithm development.

4. Spatiotemporal water clarity patterns in the Florida Keys

4.1. Analysis methods

A number of techniques were utilized to investigate the spatial and temporal variability of K_d (derived using the modified K_d_Lee) in the Florida Keys region. Variation in K_d at 488 nm is used in this analysis

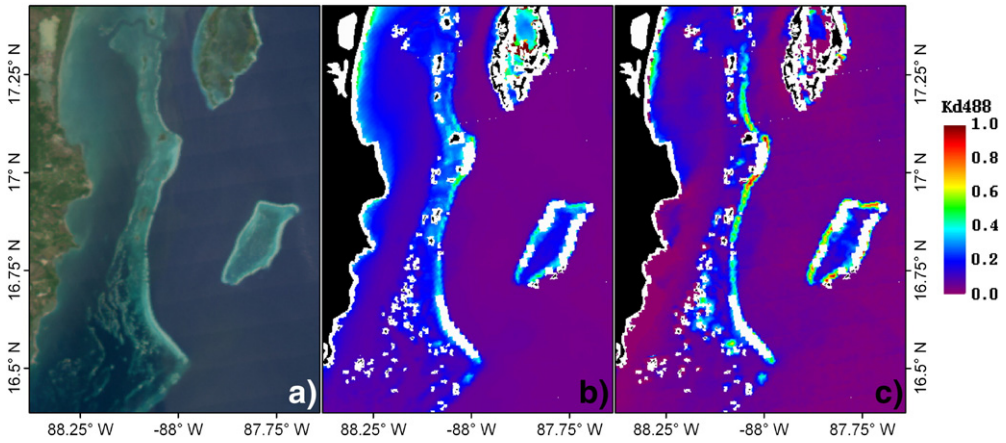

Fig. 7. MODIS/A data from 24 January 2010 covering of a portion of the Belize Barrier Reef, displayed as a) true-color image and processed to $K_d(488; m^{-1})$ using b) the standard K_d_Lee algorithm and c) the modified K_d_Lee.

because historically $K_d(490)$ or $K_d(488)$ has been used as a measure of water clarity. Light at 488 nm is within the transparency window for most waters, allowing light to reach the benthos in the FRT region.

To visualize temporal water clarity variations in this region, the monthly summaries of K_d statistics were investigated along an approximate 10 m bathymetric isobath, derived from a raster bathymetry created by Palandro (2006). For each pixel along this transect, monthly mean K_d from each month of MODIS/A data (July 2002 to Dec 2011) were extracted. This same data extraction was implemented for K_d monthly anomaly, standard deviation, and coefficient of variation data.

An empirical orthogonal function (EOF) analysis was used to explore spatiotemporal groupings in water clarity. The singular value decomposition method was used for computational efficiency (Kelly, 1988). Using ENVI (version 4.8; Exelis Visual Information Solutions) and the raster bathymetry, a region of interest (ROI) was created which included only waters south and east of the Florida Keys/Dry Tortugas and with depths of 5 to 30 m, roughly corresponding to the FRT extent. Monthly climatology data within this ROI were sorted into ASCII text files along with their latitude and longitude. As the EOF analysis requires no gaps in data coverage, any pixel without monthly climatology data for every month was excluded. The EOF was then performed on this gridded time series, resulting in twelve principal component axes (modes). Using the retained latitude and longitude, the pixel distances along each mode was color coded, re-mapped to the original position and saved as PNG files. Also recorded was the percentage of total variation described by each mode (eigenvalue), as well as the time series of monthly relative amplitudes of the data within the mode.

Finally, a two-way ANOVA was performed using Matlab® (version 2011a; MathWorks®) to evaluate regional variation in water clarity across the FRT regions (see Fig. 10). The independent variables for this test were groupings by region (Biscayne Bay, Upper, Middle and Lower Keys, Marquesas, and Dry Tortugas) and by linear distance to the closest land pixel. Linear distance from land was binned into groups 0–4 km, 4–8 km, and 8–12 km, and only waters with bottom depths of 5–30 m were considered. The dependent variable was the average of all (2002–2011) $K_d(488)$ data at each pixel. Lilliefors and Kruskal–Wallis tests were performed to assess data conformation to ANOVA assumptions of normality and homoscedasticity, respectively. Although many groups showed failure to meet one or both of these assumptions, the large number of data points and robustness of the ANOVA in such situations (Sokal & Rohlf, 1981) allowed for its appropriate implementation. The null hypothesis of this test was equal water clarity across regions and with distance from shore. Tukey's pairwise comparisons were performed to elucidate significant differences between individual groups.

4.2. Spatiotemporal patterns

The time series of climatology images (Fig. 5) show that clear water persists throughout the year for most of the region, with $K_d(488)$ generally less than 0.5 m^{-1}. The main gradient in water clarity is from high inshore to low offshore. Spring and summer months have the clearest waters, while winter months have the highest $K_d(488)$ regionally.

Along the 10 m transect, mean monthly data (Fig. 8b) again show extremely clear waters in the Upper and Middle Keys, as well as some of the same seasonal variation described above. The Upper Keys region has the clearest waters, with water clarity decreasing and becoming more variable (Fig. 8d) westward along the transect. Coefficient of variation (Fig. 8e) shows consistent scale and variability throughout time along this transect, indicating that $K_d(488)$ variability is strongly correlated to the mean $K_d(488)$.

The EOF analysis was performed so that variation within this complex system could be summarized. Mode one of the EOF explained over 85% of the variation, and its eigenvector amplitudes by month indicated that this represents a smooth seasonal cycle. EOF mode two explained 9% of the total variance, and all other modes explain less than 1.1%. With this quantity of data (over 56,000 pixels during each of 12 months), 1000 EOF analyses performed on randomly generated noise indicated that with 95% confidence, modes with eigenvalues explaining 9% or less of the variation are non-significant. Thus all modes except mode one (the seasonal cycle) were considered non-significant. As a result, a simple harmonic equation was fit to the data to describe the seasonal cycle elucidated by EOF mode one. At each pixel, the sum of squares was minimized to best fit a simple harmonic oscillation:

$$x = \overline{x} + A\cos(2\pi * t/12) + B\sin(2\pi * t/12), \quad (10)$$

where x is the satellite-derived climatology mean $K_d(488)$ from a particular month and pixel, $\overline{x}$ is the average of monthly climatologies at that pixel, t is time in months, and A and B are the pixel-specific coefficients being fit. From this harmonic equation, the amplitude $[(A^2 + B^2)^{0.5}]$ and phase $[\tan^{-1}(B,A)]$ of the oscillation were calculated and mapped (Fig. 9). In this visualization, amplitude represents one-half of the range of best-fit $K_d(488)$ values, and phase shows the timing (in months) of the maximum of this harmonic.

Finally, the two-way ANOVA showed significant effects of both region ($F = 3651$; $p < 0.0001$) and distance from shore ($F = 10290$; $p < 0.0001$) but also indicated a significant interaction ($F = 458$; $p < 0.0001$) between these two factors. As such, individual one-way ANOVAs were performed on data from each of the factor group levels. Within each region, there was a strongly significant effect of distance from land (ANOVAs for each region showed $F > 700$ with 2 d.f. and

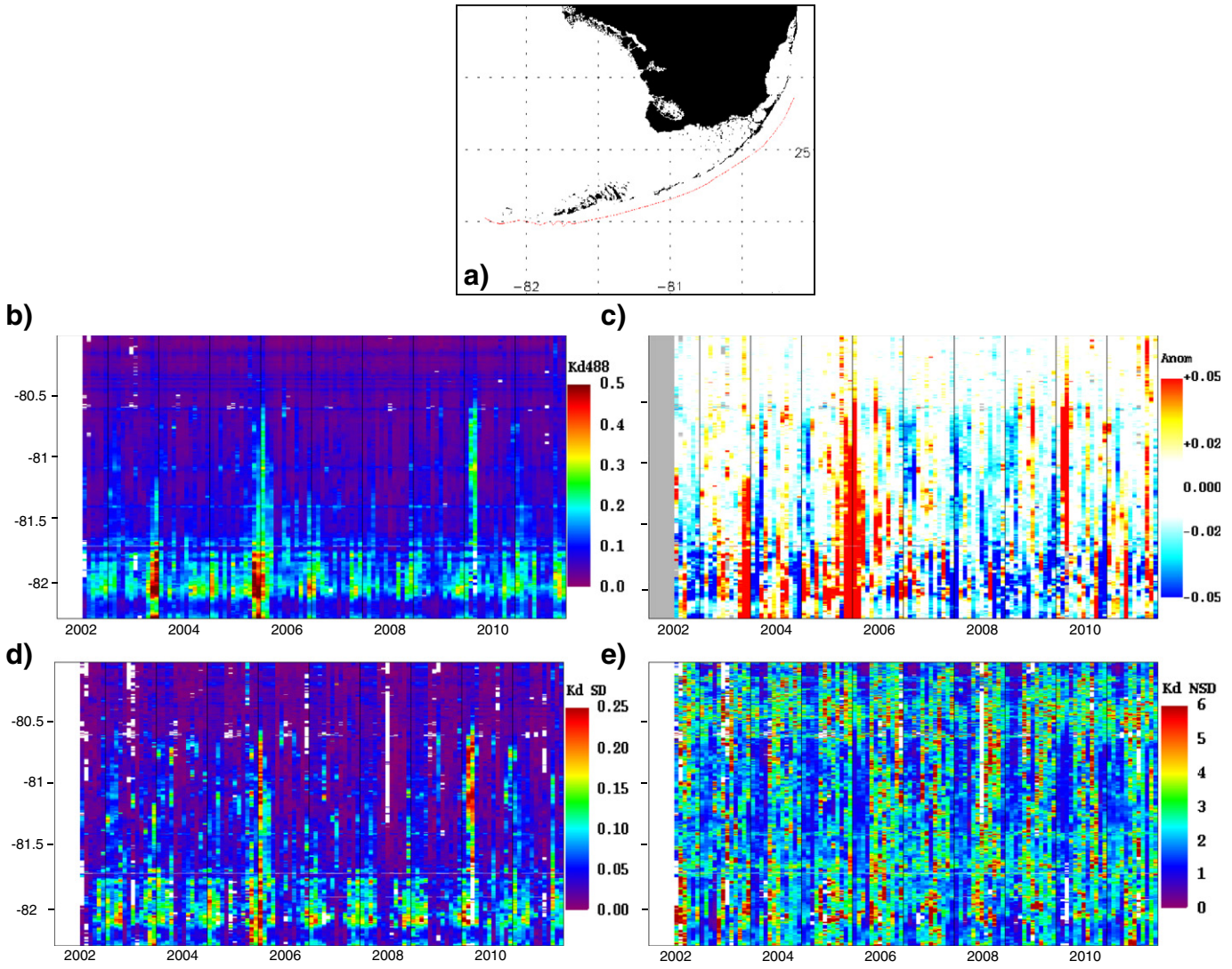

Fig. 8. Time series of monthly modified K_d_Lee(488) products for the 10-m transect along the FRT (red line) in a). The products include b) monthly mean, c) anomaly, d) standard deviation, and e) coefficient of deviation. Time (months and years) oriented on x-axis, with longitudinal position along transect displayed on y-axis.

$p < 0.0001$), and a common trend of decreasing $K_d(488)$ with distance from land. Pairwise comparisons on each regional analysis showed that each grouping by distance from land was significantly different (*i.e.*, the 0–4 km pixels within a region always had significantly higher $K_d(488)$ than the 4–8 km pixels, both which also were significantly higher than the 8–12 km pixels). Holding the distance from land group constant, ANOVAs performed on individual regions also all showed strongly significant effects (d.f. = 5; $F > 800$; $p < 0.0001$ for each ANOVA; Fig. 10). For the nearshore (0–4 km) pixels, pairwise comparison indicated that each region was significantly different from all others, with the Dry Tortugas showing the lowest $K_d(488)$ and Marquesas having the highest. Excluding the Dry Tortugas region, $K_d(488)$ significantly decreased for every region in a sequential manner northwest along the FRT (Fig. 10). This general pattern was seen for both the 4–8 km and 8–12 km groups, with some exceptions (most notably, no statistically significant difference between Middle Keys and Biscayne Bay waters 4–8 km from land).

4.3. Discussion

Together, these analyses and visualizations present a picture of clear water region-wide with generally low spatiotemporal variability. Nevertheless, validated synoptic $K_d(488)$ data can be used to detect significant differences between regions. Because data were grouped according to their traditionally defined regions (Klein & Orlando, 1994) for the ANOVA analyses, direct comparison to previous works was possible. As such, we find that the widely held hypotheses of poorest water clarity in the Middle Keys region (see Lapointe & Clark, 1992) and clearest water in the Lower Keys (see Boyer & Jones, 2002; Klein & Orlando, 1994; Szmant & Forrester, 1996) need revision. This analysis, however, does find increasing water clarity (decreasing K_d) with distance from shore, in agreement with previous studies (Lapointe & Clark, 1992; Szmant & Forrester, 1996). Also, this analysis of $K_d(488)$ concurs with the conclusion of Boyer and Jones (2002) that the Marquesas region has the highest chlorophyll concentrations.

Even though some of the relative regional differences in water clarity identified in the current work differ from the results of previous analyses of water clarity (Boyer & Jones, 2002; Klein & Orlando, 1994; Lapointe & Clark, 1992; Szmant & Forrester, 1996), the noted spatiotemporal trends are in accordance with regional circulation patterns (see Lee, 2012; Lee & Smith, 2002; Lee & Williams, 1999; Lee, T., et al., 2002; Porter et al., 1999; Smith, 1994). Specifically, although there is a net flow of water southward through the channels separating the Florida Keys islands, the strongest of such transports are in the

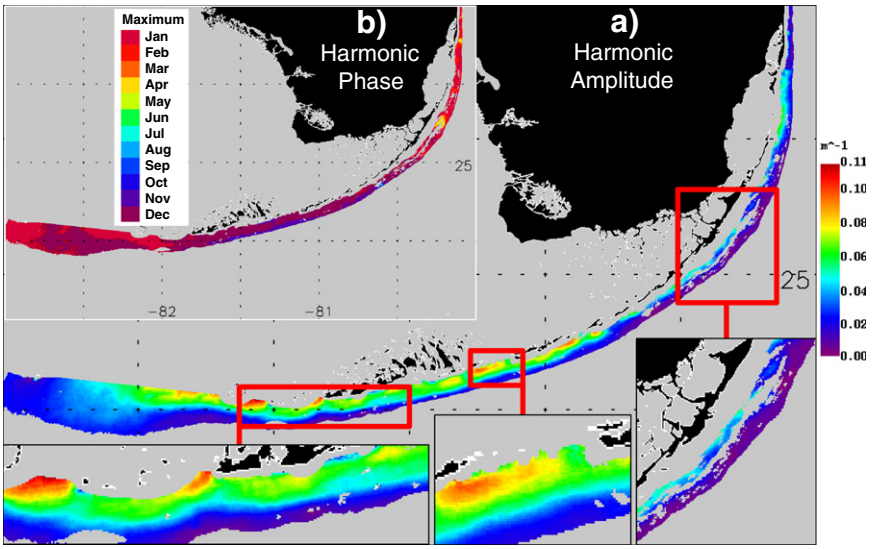

Fig. 9. EOF analysis showed singular importance of a regular seasonal cycle. Maps depict the a) amplitude and (inset map, b) phase of a simple harmonic oscillation fit to describe this cycle in $K_d(488)$ for waters with depth between 5 and 30 m. Phase is shown as month of maximum $K_d(488)$. Land shown in black with a white coastline. No data shown as gray. Inset zooms highlight representative regions from the Lower, Middle, and Upper Keys.

winter and spring (Lee., T., et al., 2002). Also, the shifting of average winds from southeasterly in the summer to easterly or northeasterly in the winter brings a reversal in flow in the Middle Keys from northward to southward (Lee, 2012). As such, in winter when the largest influxes of water are flowing into the FRT region through the Middle Keys channels, strong alongshore currents are moving this water towards the Lower Keys and Marquesas Keys regions, which can potentially explain the maxima in $K_d(488)$ noted in the Lower Keys during winter.

More importantly, however, the large quantity of data provided by MODIS/A and this modified K_d_Lee algorithm allows for more robust zonation than the traditional region designations. Within any region, sub-regions can be pinpointed which show large differences in climatology and seasonal cycle amplitude. For example, harmonic analyses showed distinct groups according to their seasonal variation, with offshore areas having the most stable water clarity (low amplitude) and inshore waters being more variable. As was seen in the mean climatologies, this is especially true in the Middle and Lower Keys, nearest the main thoroughfares for water leaving Florida Bay. The Upper Keys region appears to lack these high amplitudes in nearshore regions, which may result from a lack of large channels for water influx. Alternatively, the masking of pixels less than 5 m depth in these analyses may partially be obscuring nearshore amplitude highs in the Upper Keys. Nevertheless, the data volume provided by this method allows for testing of statistical differences between individual reef or seagrass environments, and retrospective analysis of their light exposure history.

Temporally, the EOF analysis indicated that a smooth seasonal cycle is the prevailing mechanism explaining water clarity variations. The phase of this variation shows nearly ubiquitous $K_d(488)$ maxima in the winter. November, December and January were the peak $K_d(488)$ months for 8, 69, and 18% of pixels, respectively (all other months

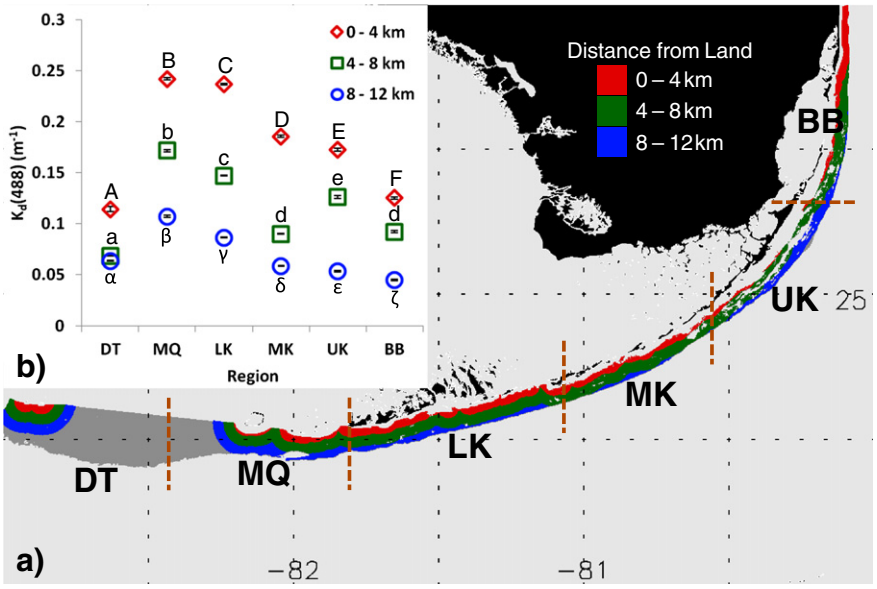

Fig. 10. ANOVA groupings and results. Underlying map (a) shows traditional regional designations, as well as groups by distance from land (red = 0–4 km, green = 4–8 km, blue = 8–12 km). Inset graph (b) shows mean ± 1 standard error for each factor level. Within each distance from land grouping, letters (capital, lower-case, or Greek) indicate regions of significant difference in pairwise comparisons. DT = Dry Tortugas, MQ = Marquesas, LK = Lower Keys, MK = Middle Keys, UK = Upper Keys, BB = Biscayne Bay.

were less than 1.5%). The Middle and Lower Keys region seems to peak earlier (November or December) than the waters to the north and to the west. Further, the time-space visualizations (Fig. 8) allow for assessment of anomalous water clarity events. The most prominent features in water clarity along the 10 m isobath are a sharp increase in mean and standard deviation of $K_d(488)$ west of approximately 81.75°W latitude (near Key West), as well as a series of low water clarity events (Fig. 8c). The former is potentially due to influxes of water from Key West and Boca Grande Channels, and agrees with other analyses showing low water clarity in the Lower Keys and Marquesas regions (Boyer & Jones, 2002). This effect could potentially be amplified by proximity to land. The 10 m transect is closer to land in the Lower Keys than in the Upper Keys, which could have the effect of capturing waters affected by land-based nutrient sources, especially the population center of Key West. Again, the ANOVA analysis showed that, regardless of region, proximity to land has a significant effect on water clarity.

The large anomalies in water clarity seen in late 2003, late 2005, and early 2010 along the 10 m isobath can be traced to particular events. First, in late 2003 a dark plume of water was observed to flow from the SW Florida coast into the Dry Tortugas region by late October (Hu et al., 2004) explaining the anomaly in derived water clarity during that time frame. The largest anomaly in water quality was seen in late 2005, due to Hurricane Wilma that passed just north of the Florida Keys in mid-October, 2005. This hurricane caused a rise in water level within Florida Bay, which overwashed most of the Middle and Lower Keys, likely leading to an extremely turbid and nutrient-rich environment. Finally, February and March of 2010 show high anomalies due to an extremely large, and previously unreported, influx of low clarity water through the channels in the Middle Keys. This plume is clearly visible in true color satellite imagery. It is possible that the extreme cold event in January 2010 (see Barnes & Hu, in press; Barnes et al., 2011; Lirman et al., 2011) caused mortality of Everglades flora and subsequent nutrient release (Duever et al., 1994). If advected into the FRT region, colored dissolved organic matter (CDOM) from the plant decay or phytoplankton blooms stimulated by the influx of nutrients could cause the anomalously high $K_d(488)$ observed.

4.4. Implications

Despite the wealth of scientific research describing the interactions between light and coral reef health, many such investigations are based on an individual coral colony (*e.g.*, Lesser et al., 1990), samplings of adult tissue (*e.g.*, Hoegh-Guldberg & Jones, 1999) or larvae microcosms (*e.g.*, Gleason et al., 2006). Unfortunately, more robust analyses are impossible because current water clarity datasets are insufficient to quantitatively assess long-term and region-wide light availability. Further, current datasets are mostly derived from long-term monitoring programs or from submerged sensor arrays, both of which are expensive and labor intensive. The algorithm described in this work adds an unprecedented amount of historical and ongoing information about the water clarity in coral reef environments, with minimal additional cost. Combined with bottom depth and satellite-derived E_d, the multispectral light environment surrounding corals can be estimated from CZCS, SeaWiFS, MODIS, MERIS, and VIIRS data using this modified algorithm, although performance may be limited by the signal-to-noise ratio of the particular instrument. As a result, the relative paucity of *in situ* light attenuation data may no longer be a factor hindering our understanding of region-wide effects of light on corals at >5 m water depth, at least for the Florida Keys.

To date, large scale investigations of declines in coral reef health have focused almost singularly on sea surface temperature (SST; *e.g.*, Liu et al., 2005). This is driven partially by the large impact of temperature on coral health, but also by the widespread availability of validated satellite SST data (as opposed to K_d data). The modified water clarity algorithm allows more robust understanding of the individual and combined effects of specific light and temperature events on corals, as well as the impacts of long-term exposures. Such information could be used to create a metric for coral health which could be assessed using satellite data in near real time.

Beyond scientific applications for the algorithm itself, the spatiotemporal patterns of water clarity in the FRT region are significant in that they depart from current conceptions about the region. The new paradigm offered in this paper describes a mainly onshore-offshore gradient in water clarity throughout the region, but also transitions in both water clarity and variability along the reef tract. As generally understood, the large discharge channels from Florida Bay greatly affect FRT waters, and indeed are driving the separation between these regions or sub-regions. Their impact is spread throughout much of the Middle and Lower Keys regions, as well as the Marquesas region.

Applied to current monitoring efforts and to the ongoing rezoning process for the FKNMS, these new satellite-based water clarity results can have significant impacts. The overall goal of these programs is to preserve native resources. Even in the absence of detailed information about the region wide impacts of current and long-term exposure to specific light regimes, the regional differences in FRT water clarity can inform these preservation efforts. Specific zones for preservation or restoration should include reefs within extremely clear waters, where corals have traditionally thrived, but also reefs acclimated to water clarity regimes which are more variable and highly attenuating (particularly nearshore). In the FKNMS, reefs in such environments currently exhibit significantly higher coral cover and coral growth rates than those in traditional offshore environments (Lirman & Fong, 2007), and as such may show resilience to potential future water clarity variability.

5. Conclusion

We have tested a modified algorithm which shows improvement in satellite derived K_d in optically shallow waters for several wavelengths, allowing widespread current and historical assessment of the light environment experienced by benthic ecosystems. This new product can further be used to investigate spatiotemporal patterns in water clarity. Within the FRT region in the Florida Keys, such analysis challenges some published accounts describing the relative clarity of the traditional geographic regions, which can have large and immediate impacts on the management of shallow marine systems. Research and monitoring efforts will benefit from combining satellite-based temperature data with this new water clarity data to allow widespread assessment of coral reef and seagrass environments in near-real time.

Acknowledgments

This work was supported by the U.S. National Aeronautics and Space Administration through its Decision Support program, Gulf of Mexico program, Ocean Biology and Biogeochemistry program, and Water and Energy Cycle program. The authors wish to thank Caiyun Zhang (Xiamen University, China) for providing the EOF routines and Gary Mitchum (University of South Florida) for assistance in EOF and harmonic oscillation analyses, as well as the anonymous reviewers whose comments helped to greatly improve this work. Coastline shape files were acquired from the NOAA National Geophysical Data Center (Wessel & Smith, 1996) and the Florida Fish and Wildlife Conservation Commission.

References

Abram, N. J., Gagan, M. K., McCulloch, M. T., Chappell, J., & Hantoro, W. S. (2003). Coral reef death during the 1997 Indian Ocean Dipole linked to Indonesian wildfires. *Science*, *301*, 952–955.

Andréfouët, S., Berkelmans, R., Odriozola, L., Done, T., Oliver, J., & Müller-Karger, F. (2002). Choosing the appropriate spatial resolution for monitoring coral bleaching events using remote sensing. *Coral Reefs*, *21*, 147–154.

Ayoub, L. M., Hallock, P., Coble, P. G., & Bell, S. S. (2012). MAA-like absorbing substances in Florida Keys phytoplankton vary with distance from shore and CDOM: Implications for coral reefs. *Journal of Experimental Marine Biology and Ecology*, *420–421*, 91–98.

Baith, K., Lindsay, R., Fu, G., & McClain, C. R. (2001). Data analysis system developed for ocean color satellite sensors. *EOS. Transactions of the American Geophysical Union*, *82*, 202.

Barnes, B. B., & Hu, C. (2013). A hybrid cloud detection algorithm to improve MODIS sea surface temperature data quality and coverage over the Eastern Gulf of Mexico. *IEEE Transactions on Geoscience and Remote Sensing*. http://dx.doi.org/10.1109/TRGS.2012.2223217 (in press).

Barnes, B. B., Hu, C., & Muller-Karger, F. (2011). An improved high-resolution SST climatology to assess cold water events off Florida. *IEEE Geoscience and Remote Sensing Letters*, *8*, 769–773.

Boyer, J. N., & Briceno, H. O. (2011). *2010 Annual Report of the Water Quality Monitoring Project for the Water Quality Protection Program of the Florida Keys National Marine Sanctuary*. Miami, FL: Southeast Environmental Research Center, Florida International University.

Boyer, J. N., & Jones, R. D. (2002). A view from the bridge: external and internal forces affecting the ambient water quality of the Florida Keys National Marine Sanctuary (FKNMS). In J. W. Porter, & K. G. Porter (Eds.), *The Everglades, Florida Bay, and coral reefs of the Florida Keys: An ecosystem sourcebook* (pp. 609–628). Boca Raton, FL: CRC Press.

Brown, B. E. (1997). Coral bleaching: causes and consequences. *Coral Reefs*, *16*, S129–S138.

Cannizzaro, J. P., & Carder, K. L. (2006). Estimating chlorophyll a concentrations from remote-sensing reflectance in optically shallow waters. *Remote Sensing of Environment*, *101*, 13–24.

Carder, K., Cannizzaro, J. P., & Lee, Z. (2005). Ocean color algorithms in optically shallow waters: Limitations and improvements. In R. J. Frouin, M. Babin, & S. Sathyendranath (Eds.), *Proc. SPIE, 5885*, Remote Sensing of the Coastal Oceanic Environment, 588506 (August 22, 2005). http://dx.doi.org/10.1117/12.615039.

Causey, B. D. (2002). The role of the Florida Keys National Marine Sanctuary in the South Florida Ecosystem Restoration Initiative. In J. W. Porter, & K. G. Porter (Eds.), *The Everglades, Florida Bay, and coral reefs of the Florida Keys: An ecosystem source book* (pp. 883–894). Boca Raton, FL: CRC Press.

Douglas, A. E. (2003). Coral bleaching—how and why? *Marine Pollution Bulletin*, *46*, 385–392.

Duever, M. J., Meeder, J. F., Meeder, L. C., & McCollom, J. M. (1994). The climate of South Florida and its role in shaping the Everglades ecosystem. In S. Davis, & J. Ogden (Eds.), *Everglades: The ecosystem and its restoration* (pp. 225–290). Boca Raton, FL, USA: St. Lucie Press.

Fisk, D. A., & Done, T. J. (1985). Taxonomic and bathymetric patterns of bleaching in corals, Myrmidon Reef (Queensland). *Proc 5th Intl Coral Reef Congr, vol. 6*. (pp. 149–154).

Foyer, C. H., Lelandais, M., & Kunert, K. J. (1994). Photooxidative stress in plants. *Physiologia Plantarum*, *92*, 696–717.

Gleason, D., Edmunds, P., & Gates, R. (2006). Ultraviolet radiation effects on the behavior and recruitment of larvae from the reef coral *Porites astreoides*. *Marine Biology*, *148*, 503–512.

Gordon, H. R., & Morel, A. Y. (1983). *Remote assessment of ocean color for interpretation of satellite visible imagery: A review*. New York: Springer-Verlag.

Hallock, P., & Schlager, W. (1986). Nutrient excess and the demise of coral reefs and carbonate platforms. *Palaios*, *1*, 389–398.

Hemminga, M. A. (1998). The root/rhizome system of seagrasses: An asset and a burden. *Journal of Sea Research*, *39*, 183–196.

Hochberg, E. J., Atkinson, M. J., & Andréfouët, S. (2003). Spectral reflectance of coral reef bottom-types worldwide and implications for coral reef remote sensing. *Remote Sensing of Environment*, *85*, 159–173.

Hoegh-Guldberg, O. (1999). Climate change, coral bleaching and the future of the world's coral reefs. *Marine and Freshwater Research*, *50*, 839–866.

Hoegh-Guldberg, O., & Jones, R. J. (1999). Photoinhibition and photoprotection in symbiotic dinoflagellates from reef-building corals. *Marine Ecology Progress Series*, *183*, 73–86.

Hooker, S. B., Lazin, G., Zibordi, G., & McLean, S. (2002). An evaluation of above- and in-water methods for determining water-leaving radiances. *Journal of Atmospheric and Oceanic Technology*, *19*, 486–515.

Hu, C. (2008). Ocean color reveals sand ridge morphology on the West Florida Shelf. *IEEE Geoscience and Remote Sensing Letters*, *5*, 443–447.

Hu, C., Hackett, K. E., Callahan, M. K., Andréfouët, S., Wheaton, J. L., Porter, J. W., et al. (2003). The 2002 ocean color anomaly in the Florida Bight: A cause of local coral reef decline? *Geophysical Research Letters*, *30*, 1151.

Hu, C., Muller-Karger, F. E., Vargo, G. A., Neely, M. B., & Johns, E. (2004). Linkages between coastal runoff and the Florida Keys ecosystem: A study of a dark plume event. *Geophysical Research Letters*, *31*.

Hu, C., Nelson, J. R., Johns, E., Chen, Z. Q., Weisberg, R. H., & Muller-Karger, F. E. (2005). Mississippi River water in the Florida Straits and in the Gulf Stream off Georgia in summer 2004. *Geophysical Research Letters*, *32*.

Hughes, T. P. (1994). Catastrophes, phase shifts, and large-scale degradation of a Caribbean Coral Reef. *Science*, *265*, 1547–1551.

Jaap, W. C. (1985). An epidemic zooxanthellae expulsion during 1983 in the lower Florida Keys coral reefs: hyperthermic etiology. *Proc. 5th Int. Coral Reef Congr., Tahiti, vol. 6*. (pp. 143–148).

Jokiel, P. L. (1980). Solar ultraviolet radiation and coral reef epifauna. *Science*, *207*, 1069–1071.

Kelble, C., & Boyer, J. N. (2007). Southern estuaries hypothesis cluster: Water quality. *Comprehensive Everglades Restoration Plan Assessment Team Final 2007 System Status Report*.

Kelly, K. A. (1988). Comment on "empirical orthogonal function analysis of advanced very high resolution radiometer surface temperature patterns in Santa Barbara Channel" by G. S. E. Lagerloef and R. L. Bernstein. *Journal of Geophysical Research*, *93*, 15753–15754.

Klein, C. J., III, & Orlando, S. P., Jr. (1994). A spatial framework for water-quality management in the Florida Keys National Marine Sanctuary. *Bulletin of Marine Science*, *54*, 1036–1044.

Lapointe, B. E., Barile, P. J., & Matzie, W. R. (2004). Anthropogenic nutrient enrichment of seagrass and coral reef communities in the Lower Florida Keys: Discrimination of local *versus* regional nitrogen sources. *Journal of Experimental Marine Biology and Ecology*, *308*, 23–58.

Lapointe, B. E., & Clark, M. (1992). Nutrient inputs from the watershed and coastal eutrophication in the Florida Keys. *Estuaries and Coasts*, *15*, 465–476.

Lee, T. N. (2012). Ocean currents connect south Florida coastal waters and link remote regions. In W. L. Kruczynski, & P. J. Fletcher (Eds.), *Tropical connections: South Florida's marine environment*. Cambridge, Maryland: IAN Press, University of Maryland Center for Environmental Science (492 pp.).

Lee, T. N., & Smith, N. (2002). Volume transport variability through the Florida Keys tidal channels. *Continental Shelf Research*, *22*, 1361–1377.

Lee, T. N., & Williams, E. (1999). Mean distribution and seasonal variability of coastal currents and temperature in the Florida Keys with implications for larval recruitment. *Bulletin of Marine Science*, *64*, 35–56.

Lee, T. N., Williams, E., Wilson, D., Johns, E., & Smith, N. (2002). Transport processes linking south Florida coastal ecosystems. In J. W. Porter, & K. G. Porter (Eds.), *The Everglades, Florida Bay and coral reefs of the Florida Keys: An ecosystem sourcebook* (pp. 309–342). Boca Raton, FL: CRC Press.

Lee, Z., Carder, K. L., & Arnone, R. A. (2002). Deriving inherent optical properties from water color: A multiband quasi-analytical algorithm for optically deep waters. *Applied Optics*, *41*, 5755–5772.

Lee, Z., Carder, K. L., Mobley, C. D., Steward, R. G., & Patch, J. S. (1999). Hyperspectral remote sensing for shallow waters. 2. Deriving bottom depths and water properties by optimization. *Applied Optics*, *38*, 3831–3843.

Lee, Z., Darecki, M., Carder, K. L., Davis, C. O., Stramski, D., & Rhea, W. J. (2005). Diffuse attenuation coefficient of downwelling irradiance: An evaluation of remote sensing methods. *Journal of Geophysical Research — Oceans*, *110*.

Lee, Z., Lubac, B., Werdell, J., & Arnone, R. (2009). *An update of the quasi-analytical algorithm (QAA_v5)*.

Lesser, M. P., & Lewis, S. (1996). Action spectrum for the effects of UV radiation on photosynthesis in the hermatypic coral *Pocillopora damicornis*. *Marine Ecology Progress Series*, *134*, 171–177.

Lesser, M. P., Stochaj, W. R., Tapley, D. W., & Shick, J. M. (1990). Bleaching in coral reef anthozoans: Effects of irradiance, ultraviolet radiation, and temperature on the activities of protective enzymes against active oxygen. *Coral Reefs*, *8*, 225–232.

Lirman, D., & Fong, P. (2007). Is proximity to land-based sources of coral stressors an appropriate measure of risk to coral reefs? An example from the Florida Reef Tract. *Marine Pollution Bulletin*, *54*, 779–791.

Lirman, D., Schopmeyer, S., Manzello, D., Gramer, L. J., Precht, W. F., Muller-Karger, F., et al. (2011). Severe 2010 cold-water event caused unprecedented mortality to corals of the Florida Reef Tract and reversed previous survivorship patterns. *PLoS One*, *6*, e23047.

Liu, G., Strong, A. E., Skirving, W., & Arzayus, L. F. (2005). Overview of NOAA coral reef watch program's near-real time satellite global coral bleaching monitoring activities. *Proc 10th Int Coral Reef Symp, vol. 1*. (pp. 1783–1793).

Lyzenga, D. R. (1981). Remote sensing of bottom reflectance and water attenuation parameters in shallow water using aircraft and Landsat data. *International Journal of Remote Sensing*, *2*, 71–82.

Maritorena, S. (1996). Remote sensing of the water attenuation in coral reefs: A case study in French Polynesia. *International Journal of Remote Sensing*, *17*, 155–166.

Maritorena, S., Morel, A., & Gentili, B. (1994). Diffuse reflectance of oceanic shallow waters: Influence of water depth and bottom albedo. *Limnology and Oceanography*, *39*, 1689–1703.

Mobley, C. D., & Sundman, L. K. (2003). Effects of optically shallow bottoms on upwelling radiances: Inhomogeneous and sloping bottoms. *Limnology and Oceanography*, *48*, 329–336.

Moore, K. A., & Wetzel, R. L. (2000). Seasonal variations in eelgrass (*Zostera marina* L.) responses to nutrient enrichment and reduced light availability in experimental ecosystems. *Journal of Experimental Marine Biology and Ecology*, *244*, 1–28.

Morel, A. (1974). Optical properties of pure water and sea water. In N. G. Jerlov, & S. Nielsen (Eds.), *Optical aspects of oceanography* (pp. 1–24). New York: Academic.

Mueller, J. L. (2000). SeaWiFS algorithm for the diffuse attenuation coefficient, K(490), using water-leaving radiances at 290 and 555 nm. In S. B. Hooker (Ed.), *SeaWiFS postlaunch calibration and validation analyses, part 3* (pp. 24–27).

National Oceanic and Atmospheric Administration (2012). *Florida Keys National Marine Sanctuary marine zoning and regulatory review, summary of scoping comments*. : Office of National Marine Sanctuaries, National Oceanic and Atmospheric Administration.

National Oceanic and Atmospheric Association (2007). *Florida Keys National Marine Sanctuary revised management plan*. : National Ocean Service, US Department of Commerce.

Ortner, P. B., Lee, T. N., Milne, P. J., Zika, R. G., Clarke, M. E., Podesta, G. P., et al. (1995). Mississippi River flood waters that reached the Gulf Stream. *Journal of Geophysical Research*, *100*, 13595–13601.

Palandro, D. (2006). Coral Reef Habitat Change and Water Clarity Assessment (1984–2002) for the Florida Keys National Marine Sanctuary Using Landsat Satellite Data. Doctoral Dissertation, College of Marine Science (p. 128). St Petersburg, FL: University of South Florida.

Palandro, D. A., Andrefouet, S., Hu, C., Hallock, P., Muller-Karger, F. E., Dustan, P., et al. (2008). Quantification of two decades of shallow-water coral reef habitat decline in

the Florida Keys National Marine Sanctuary using Landsat data (1984–2002). *Remote Sensing of Environment*, *112*, 3388–3399.
Palandro, D., Andrefouet, S., Muller-Karger, F. E., & Dustan, P. (2001). Coral reef change detection using Landsats 5 and 7: a case study using Carysfort Reef in the Florida Keys. *IGARSS '01. IEEE 2001 International. Geoscience and remote sensing symposium*, *vol. 622*. (pp. 625–627).
Palandro, D., Hu, C., Andréfouët, S., & Muller-Karger, F. E. (2004). Synoptic water clarity assessment in the Florida Keys using diffuse attenuation coefficient estimated from Landsat imagery. In D. G. Fautin, J. A. Westfall, P. Cartwrigh, M. Daly, & C. R. Wyttenbach (Eds.), *Coelenterate biology 2003* (pp. 489–493). Netherlands: Springer.
Patt, F. S., Barnes, R. A., Eplee, R. E., Jr., Franz, B. A., Robinson, W. D., Feldman, G. C., et al. (2003). Algorithm updates for the fourth SeaWiFS data reprocessing. In S. B. Hooker, & E. R. Firestone (Eds.), *NASA technical memorandum 2003-206892*.
Pope, R. M., & Fry, E. S. (1997). Absorption spectrum (380–700 nm) of pure water. II. Integrating cavity measurements. *Applied Optics*, *36*, 8710–8723.
Porter, J. W., Lewis, S. K., & Porter, K. G. (1999). The effect of multiple stressors on the Florida Keys coral reef ecosystem: A landscape hypothesis and a physiological test. *Limnology and Oceanography*, *44*, 941–949.
Riley, G. A. (1956). Oceanography of Long Island Sound, 1952–1954. II. Physical oceanography. *Bulletin of the Bingham Oceanographic Collection*, *15*, 15–46.
Rodhe, W. (1948). Environmental requirements of fresh-water plankton algae; experimental studies in the ecology of phytoplankton. *Symbolae Botanicae Upsalienses*, *10: 1*, Uppsala: Lundequistska bokhandeln (149 pp).
Schaeffer, B. A., Hagy, J. D., Conmy, R. N., Lehrter, J. C., & Stumpf, R. P. (2011). An approach to developing numeric water quality criteria for coastal waters using the SeaWiFS satellite data record. *Environmental Science & Technology*, *46*, 916–922.
Shick, J. M., & Dunlap, W. C. (2002). Mycosporine-like amino acids and related gadusols: Biosynthesis, accumulation, and UV-protective functions in aquatic organisms. *Annual Review of Physiology*, *64*, 223–262.
Shick, J. M., Lesser, M. P., & Jokiel, P. L. (1996). Effects of ultraviolet radiation on corals and other coral reef organisms. *Global Change Biology*, *2*, 527–545.
Smith, N. P. (1994). Long-term Gulf-to-Atlantic transport through tidal channels in the Florida Keys. *Bulletin of Marine Science*, *54*, 602–609.
Smith, R. C., & Baker, K. S. (1981). Optical properties of the clearest natural waters (200–800 nm). *Applied Optics*, *20*, 177–184.
Sokal, R. R., & Rohlf, F. J. (1981). *Biometry*. New York: W.H. Freeman & Co (869 pp.).
Stumpf, R. P., Holderied, K., & Sinclair, M. (2003). Determination of water depth with high-resolution satellite imagery over variable bottom types. *Limnology and Oceanography*, *48*, 547–556.
Szmant, A. M., & Forrester, A. (1996). Water column and sediment nitrogen and phosphorus distribution patterns in the Florida Keys, USA. *Coral Reefs*, *15*, 21–41.
United States Census Bureau (2011). *Census 2010 summary file 1, Florida.* : U.S. Census Bureau.
Warner, M. E., Fitt, W. K., & Schmidt, G. W. (1999). Damage to photosystem II in symbiotic dinoflagellates: A determinant of coral bleaching. *Proceedings of the National Academy of Sciences*, *96*, 8007–8012.
Werdell, P. J., & Roesler, C. S. (2003). Remote assessment of benthic substrate composition in shallow waters using multispectral reflectance. *Limnology and Oceanography*, *48*, 557–567.
Wessel, P., & Smith, W. H. F. (1996). A global, self-consistent, hierarchical, high-resolution shoreline database. *Journal of Geophysical Research — Solid Earth*, *101*, 8741–8743.
Zepp, R. G., Shank, G. C., Stabenau, E., Patterson, K. W., Cyterski, M., Fisher, W., et al. (2008). Spatial and temporal variability of solar ultraviolet exposure of coral assemblages in the Florida Keys: Importance of colored dissolved organic matter. *Limnology and Oceanography*, *53*, 1909–1922.
Zhao, J., Barnes, B. B., Nelo, M., English, D., Lapointe, B., Muller-Karger, F., et al. (2013). Assessment of satellite-derived diffuse attenuation coefficients and euphotic depths in south Florida coastal waters. *Remote Sensing of Environment*, *131*, 38–50.